7

Passive Dynamic Autonomous Control for the Multi-locomotion Robot

Tadayoshi Aoyama[1], Kosuke Sekiyama[2], Yasuhisa Hasegawa[3], and Toshio Fukuda[4]
[1,2,4]*Nagoya University,*
[3]*University of Tsukuba*
Japan

1. Introduction

Recently, skillful motions performed by animals are realized by used of actual robots (Hirai et al., 1998; McGeer, 1990; Nakanishi et al., 2000; Raibert, 1986; Saito & Fukuda, 1997). Most of these works focused on a single type of locomotion. On the other hand, animals such as primates move in several types of locomotion form and select suitable locomotion form depending on their surroundings, situation, and purpose. For example, a gorilla has high behavior flexibility in a forest by adopting bipedal walking in a narrow space, quadrupedal walking on rough terrain and brachiation in the forest canopy. Inspired by these high mobility of an animal, we have developed an anthropoid-like "Multi-locomotion robot" that can perform several types of locomotion and choose the proper one depending on robot's needs (Fig. 1, (Fukuda et al., 2009)). A development of a multi-locomotion robot which has plural locomotion types for high mobility is one of challenging issues, because a problem is remaining in addition to research issues on humanoid robot study. That is a control architecture that synthesizes several locomotion controllers. When we consider a transition connecting one locomotion to another, two independent controllers corresponding to each locomotion type are not enough. A control algorithm that covering control properties of multiple locomotion controllers should be developed because the transition motion cannot be realized by fusing control outputs from multiple controllers. Based on this notion, we have proposed a novel control method named Passive Dynamic Autonomous Control (PDAC) (Doi et al., 2004) that realize not only a bipedal walk (Aoyama et al., 2009) but also a quadrupedal

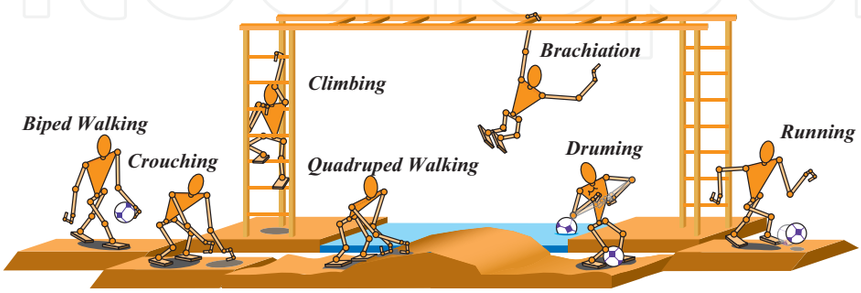

Fig. 1. Concept of the Multi-Locomotion Robot.

walk (Asano et al., 2007) and a brachiation (Fukuda et al., 2007). In this chapter, we focus on a bipedal walking control. We have already proposed 3-D biped control method based on PDAC (Aoyama et al., 2009). This chapter introduces another stabilizing method of the robot dynamics; then the stabilizing method is validated by the numerical simulation.
This chapter continues as follows. In Section 2, we introduce the Gorilla Robot III that has been developed as a prototype of the multi-locomotion robot. In Section 3, we explain about PDAC concisely. Section 4 describes the walking model, Section 5 introduces stabilization method, and Section 6 shows the results of the numerical simulation. Finally, we summarize this chapter in Section 7.

2. Multi–locomotion robot

This section introduces the "Gorilla Robot III" briefly. Gorilla robot III have been developed as a prototype of the Multi-locomotion Robot; details are found in (Fukuda et al., 2009). Figure 2 shows the overview of Gorilla Robot III and its link structure. This robot is about 1.0 m tall, weighs about 24.0 kg, and consists of 25 links and 24 AC motors including two grippers. The real-time operating system VxWorks (Wind River Systems Inc) runs on a Pentium III PC for processing sensory data and generating its behaviors. Two kinds of sensors are attached to each hand. The rate gyroscope, CRS03-04 manufactured by Silicon Sensing Systems Japan Ltd., measures the angular velocity around the contact bar to calculate the pendulum angle during the motion. The force sensor, IFS-67M25A made by NITTA CORPORATION, measures reaction forces from contact bars in order to judge whether the robot successfully grasps the bar or not.
This robot has been designed to perform biped locomotion, quadruped locomotion and brachiation. We designed the controller for all locomotion using the same algorithm "PDAC". The approach of PDAC is to describe the robot dynamics as an autonomous system around a contact point, using an interlocking so that the robot could keep the robot inherent dynamics. The PDAC is explained in next section. 3-D dynamic walking is achieved as shown in Fig.3 (Aoyama et al., 2009). We also designed a controller for a quadrupedal walk (Asano et

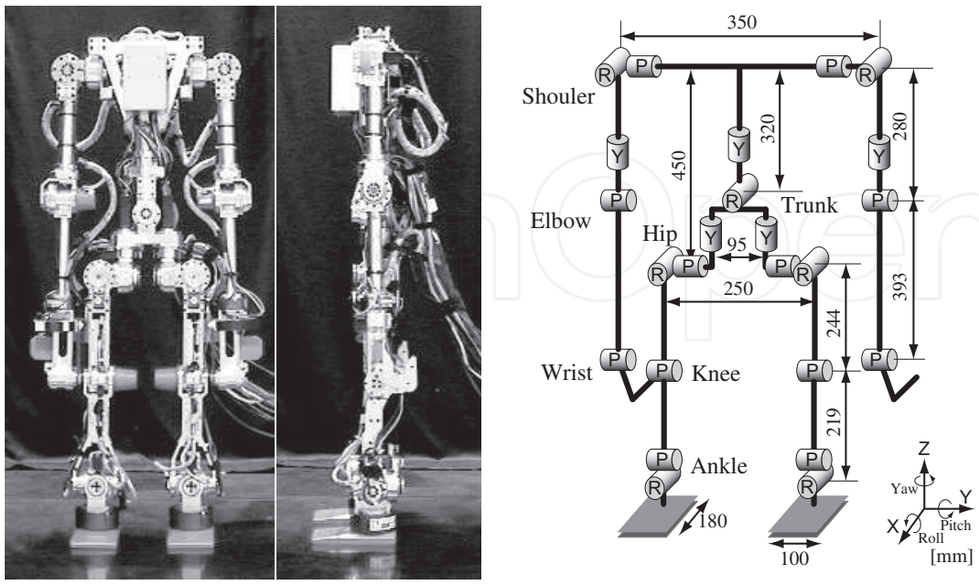

Fig. 2. Gorilla Robot III

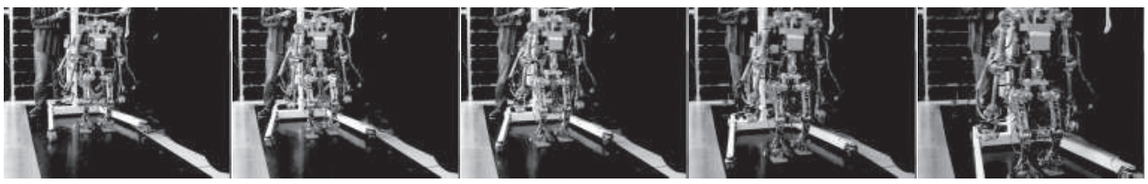

Fig. 3. Snapshots of the Bipedal Walking Experiment. Each figure shows the snapshots at (a)1st (b)7th (c)13th (d)19th (e)25th step. (Aoyama et al., 2009)

Fig. 4. Snapshots of the quadrupedal walking using PDAC. (Asano et al., 2007)

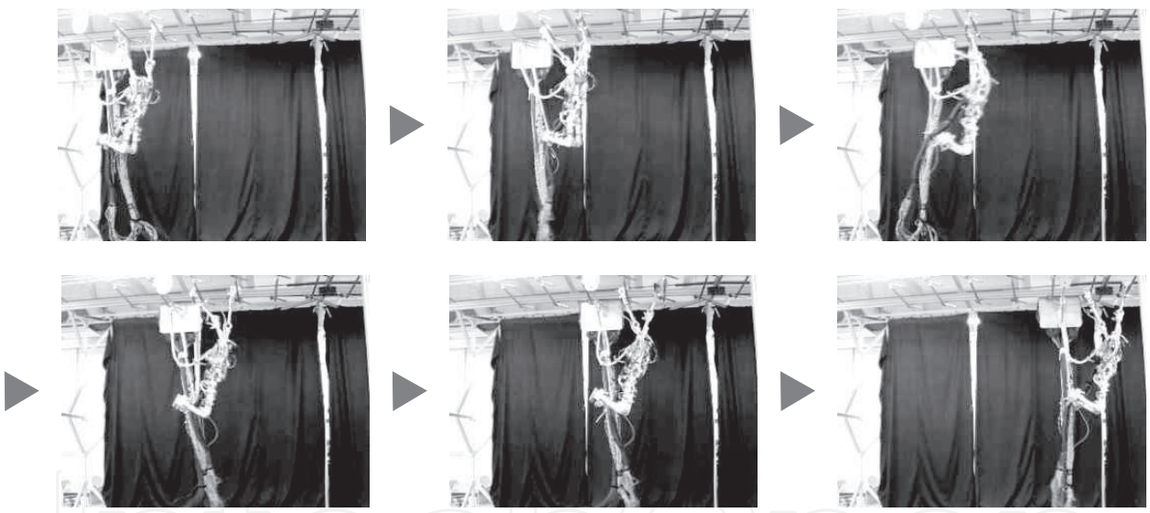

Fig. 5. Snapshots of the brachiation using PDAC. (Fukuda et al., 2007)

al., 2007), and brachiation (Fukuda et al., 2007) using the same PDAC. The snapshot of the quadrupedal walk is shown in Fig.4 and the brachiation is shown in Fig.5.

3. Passive dynamic autonomous control (PDAC)

3.1 Converged dynamics

This section gives explanation of PDAC that was proposed previously by Doi et.al. based on two concepts, i.e. the point-contact and the virtual constraint (Doi et al., 2004). The point-contact means that a robot contacts a ground at a point, that is, the first joint is passive. The virtual constraint has been proposed by Grizzle and Westervelt et al. (Grizzle et al., 2001; Westervelt et al., 2004) as a set of holonomic constraints on the robot's actuated DOF

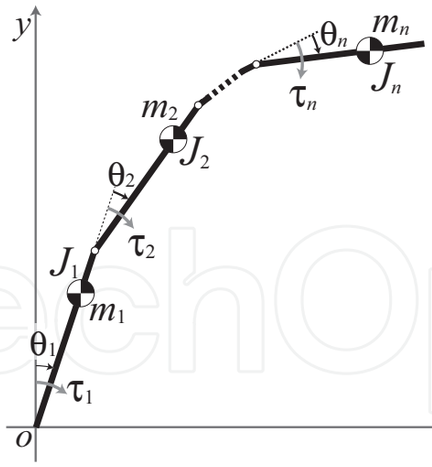

Fig. 6. Mechanical model of the serial n-link rigid robot. θ_i and τ_i are the angle and the torque of ith joint respectively. m_i and J_i are the mass and the moment of inertia of ith link respectively.

parameterized by the robot's unactuated DOF. Assuming that PDAC is applied to a serial n-link rigid robot as shown in Fig. 6, these two concepts are expressed as follows:

$$\tau_1 = 0, \tag{1}$$

$$\begin{aligned} \boldsymbol{\Theta} &= [\theta_1, \theta_2, \cdots, \theta_n]^T = [f_1(\theta), f_2(\theta), \cdots, f_n(\theta)]^T \\ &:= \boldsymbol{f}(\theta), \end{aligned} \tag{2}$$

where θ is the angle around the contact point with respect to the absolute coordinate system, that is, $\theta_1 = f_1(\theta) = \theta$.
The dynamic equations of this model are given by

$$\frac{d}{dt}\left(\boldsymbol{M}(\boldsymbol{\Theta})\dot{\boldsymbol{\Theta}}\right) - \frac{1}{2}\frac{\partial}{\partial \boldsymbol{\Theta}}\left(\dot{\boldsymbol{\Theta}}^T \boldsymbol{M}(\boldsymbol{\Theta})\dot{\boldsymbol{\Theta}}\right) - G(\boldsymbol{\Theta}) = \boldsymbol{\tau}, \tag{3}$$

where
$\boldsymbol{M}(\boldsymbol{\Theta}) := [\boldsymbol{m}_1(\boldsymbol{\Theta})^T, \boldsymbol{m}_2(\boldsymbol{\Theta})^T, \cdots, \boldsymbol{m}_n(\boldsymbol{\Theta})^T]^T$, $\boldsymbol{G}(\boldsymbol{\Theta}) := [G_1(\boldsymbol{\Theta}), G_2(\boldsymbol{\Theta}), \cdots, G_n(\boldsymbol{\Theta})]^T$, $\boldsymbol{\Theta} := [\theta_1, \theta_2, \cdots, \theta_n]^T$, $\boldsymbol{\tau} := [\tau_1, \tau_2, \cdots, \tau_n]^T$, and $\frac{\partial}{\partial \boldsymbol{\Theta}} = [\frac{\partial}{\partial \theta_1}, \frac{\partial}{\partial \theta_2}, \cdots, \frac{\partial}{\partial \theta_n}]^T$.
Since the dynamic equation around the contact point has no term of the Coriolis force in this model, it is given as

$$\frac{d}{dt}\left(\boldsymbol{m}_1(\boldsymbol{\Theta})^T\dot{\boldsymbol{\Theta}}\right) - G_1(\boldsymbol{\Theta}) = \tau_1. \tag{4}$$

By differentiating Eq. (2) with respect to time, the following equation is acquired,

$$\dot{\boldsymbol{\Theta}} = \frac{\partial \boldsymbol{f}(\theta)}{\partial \theta}\dot{\theta} = \left[\frac{\partial f_1(\theta)}{\partial \theta}, \frac{\partial f_2(\theta)}{\partial \theta}, \cdots, \frac{\partial f_n(\theta)}{\partial \theta}\right]^T \dot{\theta}. \tag{5}$$

Substituting Eqs. (1), (2) and (5) into Eq. (3) yields the following dynamic equation,

$$\frac{d}{dt}\left(M(\theta)\dot{\theta}\right) = G(\theta), \tag{6}$$

where

$$M(\theta) := \boldsymbol{m}_1 \Big(\boldsymbol{f}(\theta) \Big)^T \frac{d\boldsymbol{f}(\theta)}{d\theta}, \tag{7}$$

$$G(\theta) := G_1 \Big(\boldsymbol{f}(\theta) \Big). \tag{8}$$

By multiplying both sides of Eq. (6) by $M(\theta)\dot{\theta}$ and by integrating with respect to time, the dynamics around the contact point is obtained as follows:

$$\int \Big(M(\theta)\dot{\theta} \Big) \frac{d}{dt} \Big(M(\theta)\dot{\theta} \Big)\, dt = \int M(\theta) G(\theta) \dot{\theta}\, dt \tag{9}$$

$$\Longleftrightarrow \frac{1}{2} \Big(M(\theta)\dot{\theta} \Big)^2 = \int M(\theta) G(\theta)\, d\theta. \tag{10}$$

Therefore, the whole robot dynamics is expressed as the following one-dimensional autonomous system,

$$\dot{\theta} = \frac{1}{M(\theta)} \sqrt{2 \int M(\theta) G(\theta)\, d\theta} \tag{11}$$

$$:= \frac{1}{M(\theta)} \sqrt{2\big(D(\theta) + C\big)} \tag{12}$$

$$:= F(\theta). \tag{13}$$

In this chapter, we term Eqs. (12) and (13) as the Converged dynamics.

4. Dynamics and walking model

In this section, we describe biped walking model by means of 3-D inverted pendulum that is same as our previous work (Aoyama et al., 2009). At first, the dynamics of the model representing the robot dynamics in single-support phase is obtained. Next, by describing the pendulum length as a function of its angle, we express the whole robot dynamics as the 2-D autonomous system under the constraint that the trunk inclination is kept in the gravitational direction during the walk.

4.1 3-D inverted pendulum model

In this chapter, a robot is modeled as a 3-D inverted pendulum shown in Fig. 7(a). Since walking motion is symmetrical, the left-handed system is used in the left-leg supporting phase and vice versa as shown in Fig. 7(b) so that it is possible to describe the robot dynamics in both supporting phases as single dynamics. We apply the assumption of point-contact to this pendulum later in accordance with PDAC, hence it is possible to choose the axes of pendulum angle around contact point to express its dynamics. In this chapter, we utilize the polar coordinate system. The state variables and parameters are shown in Fig. 8(b). By use of the six variables q_1 to q_5 and l, it is possible to express any state of the robot.
Let mass of the robot be m and let tensor of inertia be

$$\boldsymbol{I} := \begin{pmatrix} I_{xx} & I_{xy} & I_{xz} \\ I_{yx} & I_{yy} & I_{yz} \\ I_{zx} & I_{zy} & I_{zz} \end{pmatrix}. \tag{14}$$

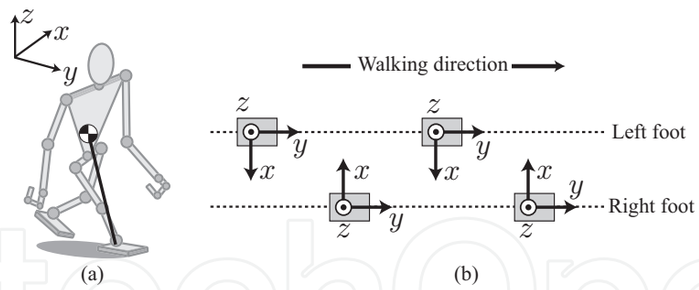

Fig. 7. (a) 3-D inverted pendulum model. (b) Definition of coordinate system. The left-handed system is used in the left-leg supporting phase and vice versa in order to facilitate the dynamics description of walking motion. Note that this figure shows just a coordinate system definition and doesn't mean that foot placement is in alignment.

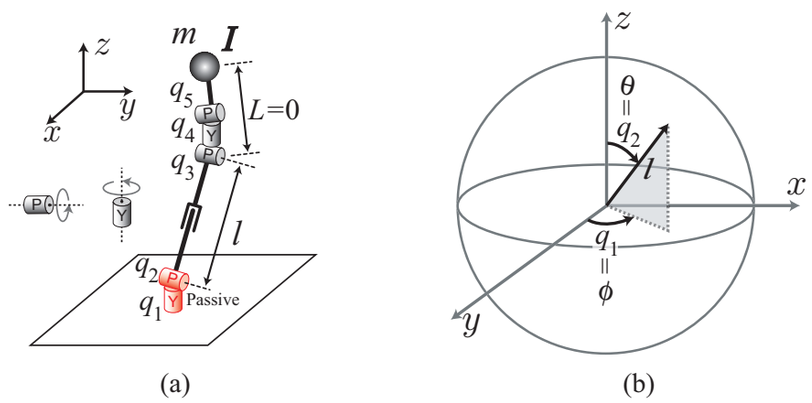

Fig. 8. (a) Parameters and variables of the 3-D inverted pendulum model. q_1 and q_2 are the variables of the pendulum angle around the contact point. q_3, q_4 and q_5 decide the upper body posture. l is the variable of the pendulum length. L is the virtual value for convenience of description and equals zero. (b) Polar coordinate system around contact point

The configuration of humanoid robots is basically symmetrical, hence generality is not lost by assuming that all products of inertia are zero, i.e. $I_{xy} = I_{yx} = I_{yz} = I_{zy} = I_{zx} = I_{xz} = 0$,

$$\begin{aligned} \boldsymbol{I} &= diag(I_{xx}, I_{yy}, I_{zz}) \\ &:= diag(I_x, I_y, I_z). \end{aligned} \tag{15}$$

Note that this tensor of inertia is parameter in the local coordinate system that is attached to the robot body, not in the global one.
In this chapter, the trunk inclination is kept in the gravitational direction and the upper body does not rotate around yaw-axis, that is,

$$q_3 = -q_2 \tag{16}$$

$$q_4 = -q_1 \tag{17}$$

$$q_5 = 0. \tag{18}$$

Then, the dynamic equations with respect to q_1, q_2, and l are obtained respectively as follows:

$$\frac{d}{dt}\left(ml^2 \sin^2 q_2 \dot{q_1}\right) = \tau_1, \tag{19}$$

$$\frac{d}{dt}\left(ml^2 \dot{q_2}\right) - ml^2 \dot{q_1}^2 \sin q_2 \cos q_2 - mgl \sin q_2 = \tau_2, \tag{20}$$

$$\frac{d}{dt}\left(m\dot{l}\right) - ml(\dot{q_1}^2 \sin^2 q_2 + \dot{q_2}^2) - mg \cos q_2 = f, \tag{21}$$

where (τ_1, τ_2, f) are the torques and force corresponding to the variables (q_1, q_2, l).

4.2 Converged dynamics

In order to control the 3-D inverted pendulum by means of PDAC, the assumption of point-contact is applied, i.e.

$$\tau_1 = \tau_2 = 0. \tag{22}$$

For simplicity of description, we describe q_1 and q_2 as ϕ and θ respectively in the below. From Eq. (16)-(22), Eq. (19) and (20) are expressed as follows:

$$\frac{d}{dt}\left(ml^2 \sin^2 \theta \dot{\phi}\right) = 0, \tag{23}$$

$$\frac{d}{dt}\left(ml^2 \dot{\theta}\right) = ml^2 \dot{\phi}^2 \sin\theta \cos\theta + mgl \sin\theta. \tag{24}$$

By multiplying both sides of Eq. (23) by $ml^2 \sin^2\theta\dot{\phi}$, and integrating with respect to time, the following constraint equation is obtained,

$$\dot{\phi} = \frac{\sqrt{2C_1}}{ml^2 \sin^2\theta} \tag{25}$$

$$:= F_1(\theta), \tag{26}$$

where C_1 is the integral constant which is decided by initial status just after foot-contact. Substituting Eq. (25) into Eq. (24) results in

$$\dot{\theta} = \frac{1}{ml^2}\sqrt{2\int\left(\frac{2C_1 \cos\theta}{\sin^3\theta} + m^2 g l^3 \sin\theta d\theta\right)} \tag{27}$$

$$:= \frac{1}{M(\theta)}\sqrt{2\big(D(\theta) + C_2\big)} \tag{28}$$

$$:= F_2(\theta). \tag{29}$$

Next, in accordance with PDAC, the pendulum length is described as the function of θ,

$$l := \lambda(\theta). \tag{30}$$

In this chapter, λ is defined as the following function of θ,

$$\lambda(\theta) =: \sqrt[3]{p_1\theta^3 + p_2\theta^2 + p_3\theta^+ p_4} \tag{31}$$

$$=: \sqrt[3]{f(\theta)}. \tag{32}$$

By substituting this equation into Eq. (28), converged dynamics is derived,

$$M(\theta) = mf(\theta)^{2/3}, \tag{33}$$

$$D(\theta) = -\frac{C_1}{\sin^2\theta} - m^2 g\Big(\big(f(\theta) - f''(\theta)\big)\cos\theta - \big(f'(\theta) - f'''(\theta)\big)\sin\theta\Big). \tag{34}$$

4.3 Design of walking cycle

In this subsection, the actual motion of the robot is designed. Figure 9 shows the schematics of the pendulum motion and the COG trajectory. The continuous line shows a trajectory of the COG in the right-leg support phase and the dotted line shows in the left-leg support phase. The dot on the edge of both the continuous line and the dotted one means a foot-contact. Figure 10 shows the parameters and variables of the pendulum motion. S_0 and S_2 denote moments just before and after a foot-contact, and S_1 is a moment at $\dot{\theta} = 0$. θ_i, ϕ_i, and l_i denote the roll angle, yaw angle, and pendulum length at S_i $(i = 0, 1, 2)$ respectively. During a cycle of walking motion, ϕ is monotonically increasing. Meanwhile, θ decreases at first, and then increases, after posing for a moment at θ_1. Thus, we compartmentalize a walking cycle from a foot-contact to the next foot-contact into two phases—Phase (A): from S_0 to S_1 $(\theta < 0)$, Phase (B): from S_1 to S_2 $(\dot{\theta} > 0)$. In the phase (A), the pendulum length is constant, thus the

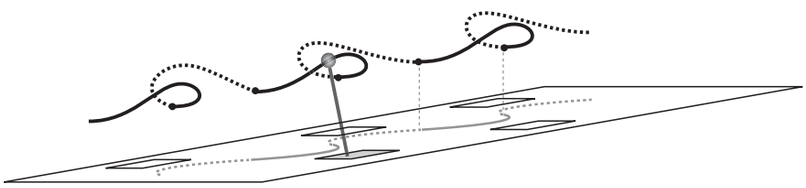

Fig. 9. Motion of the inverted pendulum. The continuous line shows the COG trajectory in the right-leg support phase and the dotted line shows in the left-leg support phase. The dot on the edge of both the continuous line and the dotted one depicts means foot-contact.

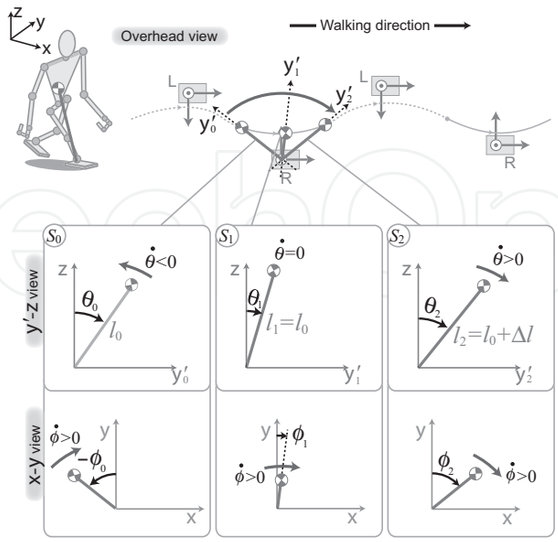

Fig. 10. Parameters and variables of dynamic walking based on 3D inverted pendulum model.

coefficients p_1-p_4 in Eq. (31) are

$$p_1 = p_2 = p_3 = 0 \tag{35}$$

$$p_d = l_0^3. \tag{36}$$

In the phase (B), the coefficients p_1-p_4 are decided so that the following four conditions are satisfied,

$$f(\theta_1) = l_1^3, \tag{37}$$

$$f(\theta_2) = l_2^3, \tag{38}$$

$$f'(\theta_2) = 0, \text{ and} \tag{39}$$

$$-f''(\theta_1)\cos\theta_1 + \left(-f'(\theta_1) + f'''(\theta_1)\right)\sin\theta_1 = 0. \tag{40}$$

Eqs. (37) and (38) signify the condition of pendulum length continuity, and Eq. (39) is the condition that the velocity of pendulum along l is 0 at a foot-contact. The objective of Eq. (40) is to match PDAC constants of the phase (A) and (B).
From Eqs. (37)-(40), the coefficients p_1-p_4 are derived as follows:

$$p_1 = -\frac{l_2^3 - l_0^3}{(\theta_2 - \theta_1)^2}\frac{u_3}{u_1 u_3 - u_2}, \tag{41}$$

$$p_2 = -\frac{l_2^3 - l_0^3}{(\theta_2 - \theta_1)^2}\frac{u_2}{u_1 u_3 - u_2}, \tag{42}$$

$$p_3 = -3p_1\theta_2^2 - 2p_2\theta_2, \text{ and} \tag{43}$$

$$p_4 = l_2^3 - p_1\theta_2^3 - p_2\theta_2^2 - p_3\theta_2, \tag{44}$$

where

$$u_1 = 2\theta_2 + \theta_1, \tag{45}$$

$$u_2 = -6\theta_1\cos\theta_1 - 3\theta_1^2\sin\theta_1 + 6\sin\theta_1 + 3\theta_2^2\sin\theta_1, \text{and} \tag{46}$$

$$u_3 = -2\cos\theta_1 - 2\theta_1\sin\theta_1 + 2\theta_2\sin\theta_1. \tag{47}$$

4.4 Foot-contact model

In this chapter, the impact between the foot and a ground is assumed to be perfectly inelastic. Thus the angular momentum around a new contact point is conserved. Assuming that ϕ_0 is the angle of ϕ just before a foot-contact, the position vector of the pendulum after impact, $\boldsymbol{L}$ is

$$\boldsymbol{L} = [l_0\sin\phi_0\sin\theta_0, l_0\cos\phi_0\sin\theta_0, l_0\cos\theta_0]^T, \tag{48}$$

where ϕ_0 and θ_0 are angles in the coordinate system of next step.
The vector of velocity immediately prior to a foot-contact, $\boldsymbol{V_1}$, is calculated as follows:

$$\boldsymbol{V_1} = [v_x, v_y, v_z]^T, \tag{49}$$

$$\begin{aligned}
\text{where} \quad v_x &= l_2(\dot{\phi}_2\cos\phi_2\sin\theta_2 + \dot{\theta}_2\sin\phi_2\cos\theta_2) + \dot{l}_2(\sin\phi_2\sin\theta_2) \\
v_y &= l_2(-\dot{\phi}_2\sin\phi_2\sin\theta_2 + \dot{\theta}_2\cos\phi_2\cos\theta_2) + \dot{l}_2(\cos\phi_2\sin\theta_2) \\
v_z &= -l_2\dot{\theta}_2\sin\theta_2 + \dot{l}_2(\cos\theta_2),
\end{aligned}$$

where ϕ_2 is the angle of ϕ just before an impact.
The velocity vector after the impact, $\boldsymbol{V_0}$, is found by the following calculation,

$$\boldsymbol{V_0} = \frac{\boldsymbol{V_1} \cdot (\boldsymbol{L} \times (\boldsymbol{V_1} \times \boldsymbol{L}))}{|\boldsymbol{L} \times (\boldsymbol{V_1} \times \boldsymbol{L})|} (\boldsymbol{L} \times (\boldsymbol{V_1} \times \boldsymbol{L})) \tag{50}$$

$$= \frac{\boldsymbol{L} \times (\boldsymbol{V_1} \times \boldsymbol{L})}{l^2} \tag{51}$$

$$:= [v'_x, v'_y, v'_z]^T. \tag{52}$$

Note that in the above calculation of $\boldsymbol{V_0}$, $\boldsymbol{V_1}$ must be treated as $\boldsymbol{V_1} = [-v_x, v_y, v_z]$ since left- and right-handed systems are switched at the foot-contact.
From Eq. (52), $\dot{\theta}_0$ and $\dot{\phi}_0$ are decided,

$$\dot{\theta}_0 = \frac{l_2}{l_0}\Big(\dot{\phi}_2 \cos\theta_0 \sin\theta_2 \sin(\phi_0 + \phi_2) + \dot{\theta}_2\big(\sin\theta_2 \sin\theta_0 - \cos\theta_0 \cos\theta_2 \cos(\phi_0 + \phi_2)\big)\Big), \tag{53}$$

$$\dot{\phi}_0 = \frac{l_2}{l_0 \sin\theta_0}\Big(\dot{\theta}_2 \cos\theta_2 \sin(\phi_0 + \phi_2) + \dot{\phi}_2 \sin\theta_2 \cos(\phi_0 + \phi_2)\Big). \tag{54}$$

5. Stabilization

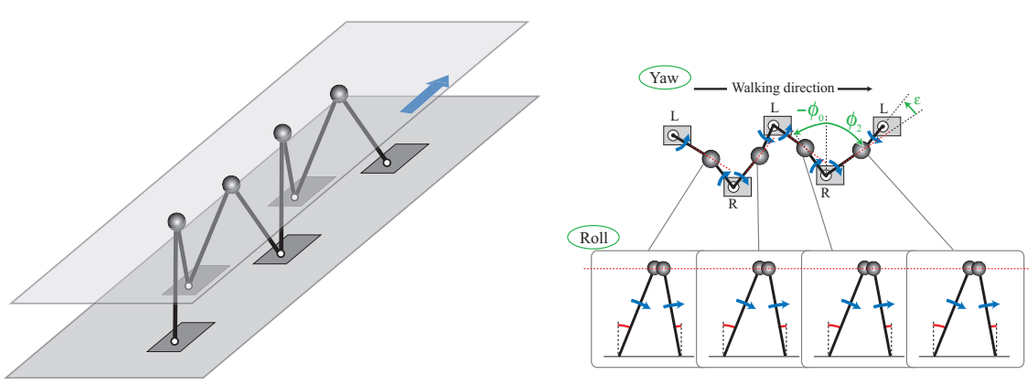

Fig. 11. Geometrical constraints at foot-contact

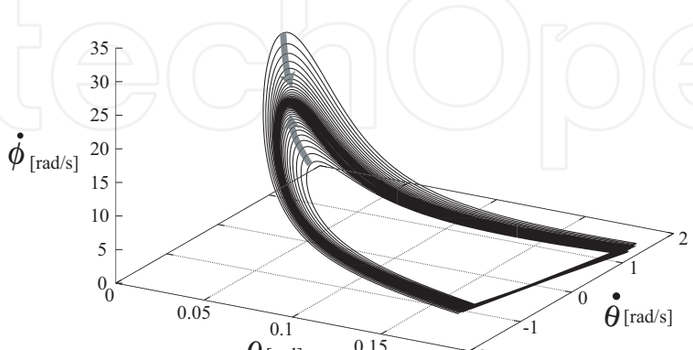

Fig. 12. Simulation results under the condition of ϵ=0.018[rad]=const, l_0 =0.51[m], Δl =0.007[m]

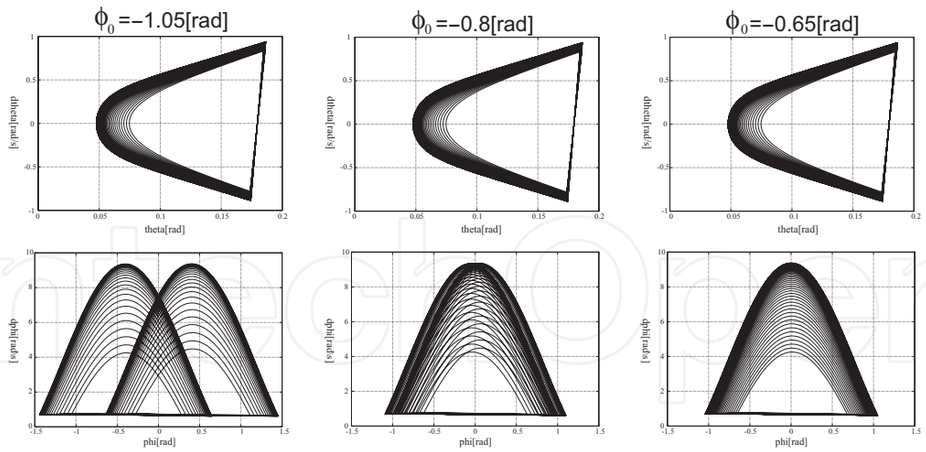

Fig. 13. Phase portrait around yaw- and roll axis under the condition of $\epsilon = \text{const}$. The three instance of various ϕ_0 is shown.

5.1 Geometrical constraints

In order to stabilize walking, some constraints are given. At first, the lengthening value of pendulum is fixed at constant value. In this constraint, supplied energy is nearly constant. In addition, the following two constraints at foot-contact, are designed as shown in Fig. 11,

- COG height h at a foot-contact is constant, i.e. roll angles of stance- and swing-leg are constant at foot-contact.
- Yaw angle of swing-leg is shifted by ϵ from the symmetrical position with stance-leg at foot-contact, i.e. it is $\phi_0[k+1] = -\phi_2[k] + \epsilon$ where $\phi_0[k+1]$ and $\phi_2[k]$ denote ϕ_0 and ϕ_2 at $k+1$th and kth step respectively.

5.2 Convergence analysis of the dynamics

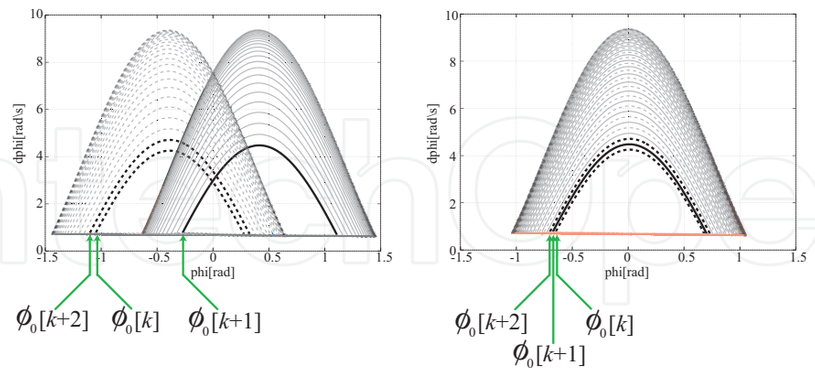

Fig. 14. Nested structure of the trajectory. $\phi_0[k]$ denotes the yaw angle at the beginning of stance-leg phase.

In this subsection, the convergence analysis is conducted. Fig. 12 depicts the simulation result under the condition of ϵ=0.018[rad]=const, l_0 =0.51[m], and Δl =0.007[m]. As can be seen in this figure, θ and $\dot{\theta}$, $\dot{\phi}$ are converged on a certain fixed point. However, it can be seen in Fig. 13, which shows the phase portrait around yaw- and roll axis, that the trajectory is not converged

on a unique one and two-cycle trajectory appears. If two-cycle occurs, a robot walks leftwards and cannot walk straight.
In this simulation, the initial angle around yaw-axis, ϕ_0, is varied without changing any other state and condition. From this figure, it can be seen that the converged trajectory seems to be depending on the initial state and that there is the certain set of initial state converging a unique trajectory.
Here, the phase portrait around yaw-axis is focused on. Fig. 14 shows the ones under the left and right condition in Fig. 13 in which the left- and right-leg supporting phases are depicted by the dotted and continuous line respectively. As shown in this figure, in the condition of unique-trajectory-convergence, the phase portrait around yaw axis possesses the nested structure, i.e. the trajectories in left- and right-leg supporting phase are nested each other—$\phi_0[k+1]$ is in between $\phi_0[k]$ and $\phi_0[k+2]$—and gradually attracted. Note that $\phi_0[k]$ is ϕ_0 value at kth step. Hence, it is contemplated that by the controller adjusting ϵ so as to achieve the nested structure of phase portrait around yaw-axis, it is possible to converge the dynamics on a unique trajectory.

5.3 Landing position control

In this subsection, we design the stabilizing controller that adjusts the landing position of stance-leg foot base on the nested structure.
If the present state is inside the converged trajectory, the condition to achieve the nested structure is described as

$$(\phi_0[k] > \phi_0[k+1]) \wedge (\phi_0[k+1] > \phi_0[k+2]). \tag{55}$$

Meanwhile, it the present state is outside, it is

$$(\phi_0[k] < \phi_0[k+1]) \wedge (\phi_0[k+1] < \phi_0[k+2]). \tag{56}$$

In order to build the stabilizing controller making the yaw dynamics attract to the nested structure, we define the distance between present state and the nested structure and design the stabilizing method minimizing this distance as follows:

$$\min(\sqrt{(\phi_0[k+2]-\phi_0[k+1])^2+(\phi_0[k+1]-\phi_0[k])^2}). \tag{57}$$

By adjusting the landing position according to this equation, it is conceivable that robot dynamics is attracted to the nested structure and consequently converged on a unique trajectory.

6. Walking simulation

The validity of proposed control was tested by numerical simulation. Fig. 15 and Fig. 16 show the simulation results of the proposed control. Fig. 15(b) depicts the result of the controller embedded the above-mentioned stabilization. In Fig. 15(a) and (b), same initial condition is employed. Note that, as shown in Fig. 15(a), the two-cycle trajectory appears without stabilization, however in Fig. 15(b), the dynamics is converged on unique trajectory with stabilization.
The proposed stabilizing method succeeded in convergence the two-cycle trajectory on a unique trajectory. Fig. 17 shows the simulation snapshots of dynamic walking control. Without stabilization based on landing position control, 3-D walking was converged on not unique trajectory but two-cycle one, hence the robot could not walk straight and walked leftwards as can be seen in Fig. 17. Meanwhile, with stabilization, it was confirmed that the

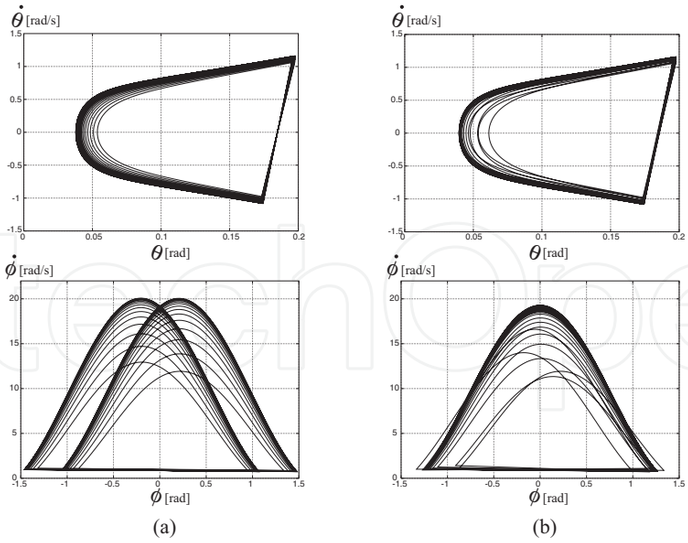

Fig. 15. Simulation results of the proposed stabilizing control.

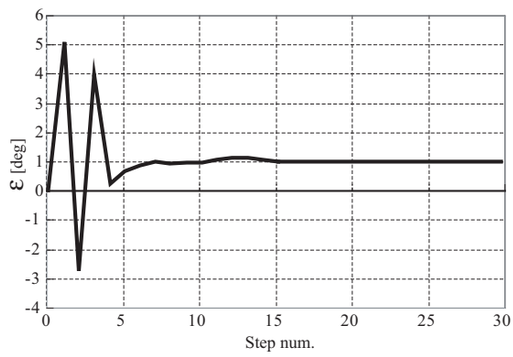

Fig. 16. Alteration of ϵ in landing position control

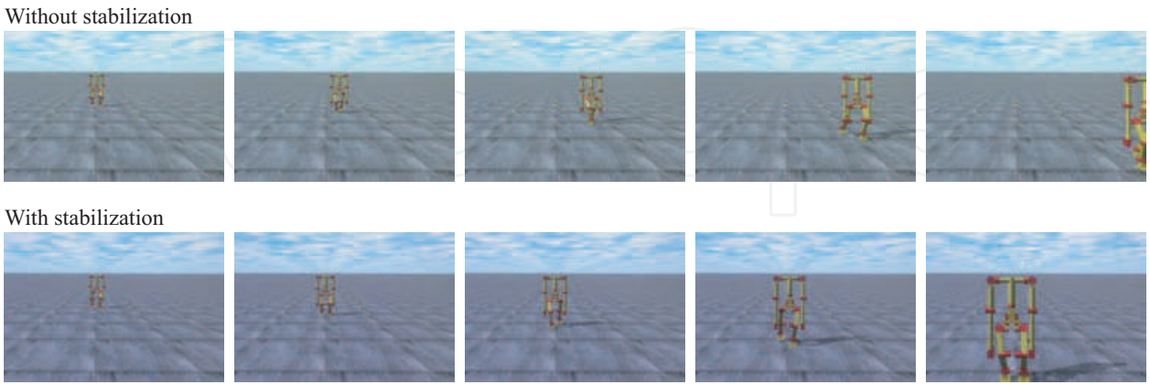

Fig. 17. Simulation snapshots of biped walking based on 3D dynamics

robot can walk straight. After convergence, step-length, walking period, and walking velocity were 0.18[m], 0.65[s], and 0.28[m/s] respectively.

7. Conclusion

In this chapter, the concept of the multi-locomotion robot that has the high mobilization capacity by achieving several kinds of locomotion independently was introduced at first. In addition, the Gorilla Robot III was introduced as hardware of the multi-locomotion robot. Second, the Passive Dynamic Autonomous Control (PDAC) which has proposed previously was explained. Not only biped walk but also quadruped walk and brachiation have been realized in our previous work. Third, we proposed the stabilizing control method that realizes 3-D biped walking based on the assumption of point-contact. The proposed method described the robot dynamics by use of a 3-D inverted pendulum model in the polar coordinate system. We applied the PDAC concept to the robot dynamics and expressed the 3-D dynamics as the 2-D autonomous system. In addition, the stabilizing controller adjusting landing position to make yaw dynamics attract to the nested structure was designed. Finally, the validity of proposed controller is tested by numerical simulation.

8. References

Aoyama, T.; Hasegawa, Y.; Sekiyama K. & FukudaT. (2009). Stabilizing and Direction Control of Efficient 3-D Biped Walking Based on PDAC. *IEEE/ASME Transactions on Mechatronics*, Vol.14, No.6, pp.712-718.

Asano, Y.; Doi, M.; Hasegawa, Y.; Matsuno, T. & Fukuda, T. (2007). Quadruped Walking by Joint-interlocking Control Based on the Assumption of Point-contact. *Transactions of the Japan Society of Mechanical Engineers, Series C*, Vol.73, No.727, pp.230-236 (in Japanese).

Doi, M.; Hasegawa, Y. & Fukuda, T. (2004b). Passive Dynamic Autonomous Control of Bipedal Walking. *Proceedings of IEEE-RAS/RSJ International Conference on Humanoid Robots*, Paper no.72, Los Angeles.

Fukuda, T.; Kojima, S.; Sekiyama, K. & Hasegawa, Y. (2007). Design Method of Brachiation Controller based on Virtual Holonomic Constraint. *Proceedings of the IEEE/RSJ International Conference on Intelligent Robots and Systems*, pp.450-455, San Diego.

Fukuda, T.; Aoyama, T.; Hasegawa, Y. & Sekiyama, K. (2009). Multilocomotion Robot:Novel Concept, Mechanism, and Control of Bio-inspired Robot. *Arti□cial Life Models in Hardware*, pp. 65-86, Springer-Verlag.

Grizzle, J. W.; Abba, G. & Plestan, F. (2001). Asymptotically Stable Walking for Biped Robots: Analysis via Systems with Impulse Effects. *IEEE Transactions on Automatic Control*, Vol.46, No.1, pp.56-64.

Hirai, K.; Hirose, M.; Haikawa, Y. & Takenaka, T. (1998). The Development of Honda Humanoid Robot. *Proceedings of the IEEE International Conference on Robotics and Automation*, pp.1321-1326, Leuven.

McGeer, T. (1990). Passive dynamic walking. *The International Journal of Robotics Research*, Vol.9, No.2, pp.62-82.

Nakanishi, J.; Fukuda, T. & Koditschek, D.E. (2000). A brachiating robot controller. *IEEE Transactions on Robotics and Automation*, Vol.16, No.2, pp.109-123.

Raibert, M.H.; (1986). Legged Robots that Balance. Cambridge, MA:MIT Press.

Saito, F.; & Fukuda, T. (1997). A First Result of The Brachiator III -A New Brachiation Robot Modeled on a Siamang. *Artificial Life V*, pp.354-361, Cambridge, MA:MIT Press.

Westervelt, E. R.; Buche, G. & Grizzle, J. W. (2004). Experimental Validation of a Framework for the Design of Controllers that Induce Stable Walking in Planar Bipeds. *The International Journal of Robotics Research*, Vol.24, No.6, pp.559-582.

Biped Robots

Edited by Prof. Armando Carlos Pina Filho

ISBN 978-953-307-216-6
Hard cover, 322 pages
Publisher InTech
Published online 04, February, 2011
Published in print edition February, 2011

Biped robots represent a very interesting research subject, with several particularities and scope topics, such as: mechanical design, gait simulation, patterns generation, kinematics, dynamics, equilibrium, stability, kinds of control, adaptability, biomechanics, cybernetics, and rehabilitation technologies. We have diverse problems related to these topics, making the study of biped robots a very complex subject, and many times the results of researches are not totally satisfactory. However, with scientific and technological advances, based on theoretical and experimental works, many researchers have collaborated in the evolution of the biped robots design, looking for to develop autonomous systems, as well as to help in rehabilitation technologies of human beings. Thus, this book intends to present some works related to the study of biped robots, developed by researchers worldwide.

How to reference

In order to correctly reference this scholarly work, feel free to copy and paste the following:

Tadayoshi Aoyama, Kosuke Sekiyama, Yasuhisa Hasegawa, and Toshio Fukuda (2011). Passive Dynamic Autonomous Control for the Multi-Locomotion Robot, Biped Robots, Prof. Armando Carlos Pina Filho (Ed.), ISBN: 978-953-307-216-6, InTech, Available from: http://www.intechopen.com/books/biped-robots/passive-dynamic-autonomous-control-for-the-multi-locomotion-robot

INTECH
open science | open minds

InTech Europe
University Campus STeP Ri
Slavka Krautzeka 83/A
51000 Rijeka, Croatia
Phone: +385 (51) 770 447
Fax: +385 (51) 686 166
www.intechopen.com

InTech China
Unit 405, Office Block, Hotel Equatorial Shanghai
No.65, Yan An Road (West), Shanghai, 200040, China
中国上海市延安西路65号上海国际贵都大饭店办公楼405单元
Phone: +86-21-62489820
Fax: +86-21-62489821

IntechOpen